Inducing Immunogenic Cancer Cell Death through Oxygen-Economized Photodynamic Therapy with Nitric Oxide-Releasing Photosensitizers

Xu, Feijie; Wang, Meijun; Dotse, Eunice; Chow, Kwan T.; Lo, Pui-Chi

Published in:
Angewandte Chemie International Edition

Published: 09/09/2024

Document Version:
Final Published version, also known as Publisher's PDF, Publisher's Final version or Version of Record

Published version (DOI):
10.1002/anie.202404561

Publication details:
Xu, F., Wang, M., Dotse, E., Chow, K. T., & Lo, P.-C. (2024). Inducing Immunogenic Cancer Cell Death through Oxygen-Economized Photodynamic Therapy with Nitric Oxide-Releasing Photosensitizers. *Angewandte Chemie International Edition*, *63*(37), Article e202404561. https://doi.org/10.1002/anie.202404561

How to cite: *Angew. Chem. Int. Ed.* **2024**, *63*, e202404561
doi.org/10.1002/anie.202404561

Photodynamic Therapy

Inducing Immunogenic Cancer Cell Death through Oxygen-Economized Photodynamic Therapy with Nitric Oxide-Releasing Photosensitizers

Feijie Xu, Meijun Wang, Eunice Dotse, Kwan T. Chow, and Pui-Chi Lo**

Abstract: Photodynamic therapy (PDT) utilizes reactive oxygen species (ROS) for eradication of cancer cells. Its effectiveness is governed by the oxygen content, which is scarce in the hypoxic tumor microenvironment. We report herein two zinc(II) phthalocyanines substituted with two or four nitric oxide (NO)-releasing moieties, namely **ZnPc-2NO** and **ZnPc-4NO**, which can suppress the mitochondrial respiration, thereby sparing more intracellular oxygen for PDT. Using HT29 human colorectal adenocarcinoma cells and A549 human lung carcinoma cells, we have demonstrated that both conjugates release NO upon interaction with the intracellular glutathione, which can reduce the cellular oxygen consumption rate and adenosine triphosphate generation and alter the mitochondrial membrane potential. They can also relieve the hypoxic status of cancer cells and decrease the expression of hypoxia-inducible factor protein HIF-1α. Upon light irradiation, both conjugates can generate ROS and induce cytotoxicity even under a hypoxic condition, overcoming the oxygen-dependent nature of PDT. Interestingly, the photodynamic action of **ZnPc-2NO** elicits the release of damage-associated molecular patterns, inducing the maturation of dendritic cells and triggering an antitumor immune response. The immunogenic cell death caused by this oxygen-economized PDT has been demonstrated through a series of in vitro and in vivo experiments.

Introduction

Photodynamic therapy (PDT) utilizes reactive oxygen species (ROS) for elimination of malignant cells and tissues. These highly cytotoxic species are generated through the excitation of photosensitizers by light, followed by the interaction with the endogenous oxygen. This modality is now a clinically approved procedure for the treatment of a variety of localized and superficial cancers.[1] The treatment outcome depends largely on the tumor specificity of the photosensitizers, the oxygen concentration in the tumor microenvironment, and the efficiency of light delivery. Various approaches have been explored extensively with a view to confining the photodynamic action at the tumor site, thus reducing the unwanted photodamage.[2] In particular, the active-targeting and activatable strategies have been integrated to further enhance the specificity of the treatment.[3] Recently, considerable efforts have been devoted to advancing the functions of photosensitizers and addressing the challenges of PDT, aiming to further improve the tumor specificity, enhance the PDT efficacy against tumor hypoxia, and devise effective strategies to circumvent the limitation of light penetration.[4]

It has been well documented that the efficacy of PDT is restricted by its dependence on oxygen, limiting its application in combating hypoxic tumors. Hypoxia is a common feature of advanced solid tumors, arising from the rapid growth of cancer cells and the disrupted vasculature, leading to inadequate oxygen delivery to the tissues.[5] Moreover, oxygen is continuously depleted during the photodynamic process, which further exacerbates the tumor hypoxia and reduces the PDT efficacy. To address this challenge, various approaches have been investigated to enrich the oxygen level in the tumor microenvironment.[6] For example, carriers such as hemoglobin and perfluorocarbons have been used to deliver oxygen to the tumor site to provide additional oxygen for PDT.[7] However, these carriers suffer from poor oxygen loading, rapid oxygen leakage, difficulty in co-delivery of other therapeutics, and the complex factors affecting oxygen release. Another strategy involves the in situ generation of oxygen, which can be achieved through catalytic transformation of the endogenous H_2O_2 into oxygen by different means.[8] These approaches, however, are limited by the low endogenous H_2O_2 level, low catalytic efficiency, and the potential toxicity of metal catalysts. Recently, an alternative strategy has been proposed that aims to inhibit the cellular respiration in order to spare more endogenous oxygen for the photodynamic action. A wide range of agents, such as nitric oxide (NO),[9] lonidamine,[10] atovaquone (ATO),[11] tamoxifen,[12]

[*] F. Xu, M. Wang, E. Dotse, K. T. Chow, P.-C. Lo
Department of Biomedical Sciences and Tung Biomedical Sciences Centre
City University of Hong Kong
Kowloon, Hong Kong (China)
E-mail: kwan.chow@cityu.edu.hk
gigi.lo@cityu.edu.hk

metformin,[13] and 7-amino carboxycoumarins-2[14] have been used for this purpose. Cellular respiration, also known as mitochondria-associated oxidative phosphorylation (OXPHOS), consumes the majority of cell's physiological oxygen.[15] It has been reported that reducing the oxygen consumption is more effective than increasing the oxygen supply in alleviating tumor hypoxia.[16]

Among the aforementioned agents, NO is of particular interest. It can inhibit the enzymatic function of cytochrome oxidase (complex IV) and suppress cellular respiration.[17] Therefore, it is a promising agent for combating tumor hypoxia. To date, several classes of NO donors have been developed, such as organic nitrates, metal-NO complexes (e.g. sodium nitroprusside, SNP), *N*-nitrosamines, and nitrosothiols.[18] NO donors are usually encapsulated in nanocarriers based on polymers or metal–organic frameworks.[9] However, the fabrication of these nanomaterials usually involves a tedious protocol, and the nanomaterials may also pose potential hazard to healthy tissues. While most of the oxygen-economized photosensitizing systems, including those containing NO donors, are in a nanostructured form, the molecular counterparts have rarely been reported so far.

Therefore, we sought to explore this approach by designing two molecular NO-releasing photosensitizers to alleviate tumor hypoxia for enhanced PDT. These conjugates consisted of a zinc(II) phthalocyanine (ZnPc) core substituted with two or four glutathione (GSH)-responsive NO donors, namely **ZnPc-2NO** and **ZnPc-4NO**, respectively. Upon internalization into cancer cells, these conjugates reacted with the enriched intracellular GSH to release NO, which could inhibit the cellular respiration, thereby reducing the oxygen consumption rate (OCR) and adenosine triphosphate (ATP) generation, eventually reversing the tumor hypoxic state. The released NO could also cause mitochondrial dysfunction and downregulation of hypoxia-inducible factor 1α (HIF-1α) for enhanced PDT. The mechanistic actions are outlined in Figure 1 using **ZnPc-2NO** as an example. Interestingly, during the course of the study, we also found that the photodynamic action of this photosensitizer could induce immunogenic cell death (ICD) of cancer cells. It induced the release of damage-associated molecular patterns (DAMPs), including calreticulin (CRT), ATP, and high-mobility group box-1 (HMGB1), triggering the maturation of dendritic cells (DCs) and the production of pro-inflammatory cytokines. The elicitation of an anti-

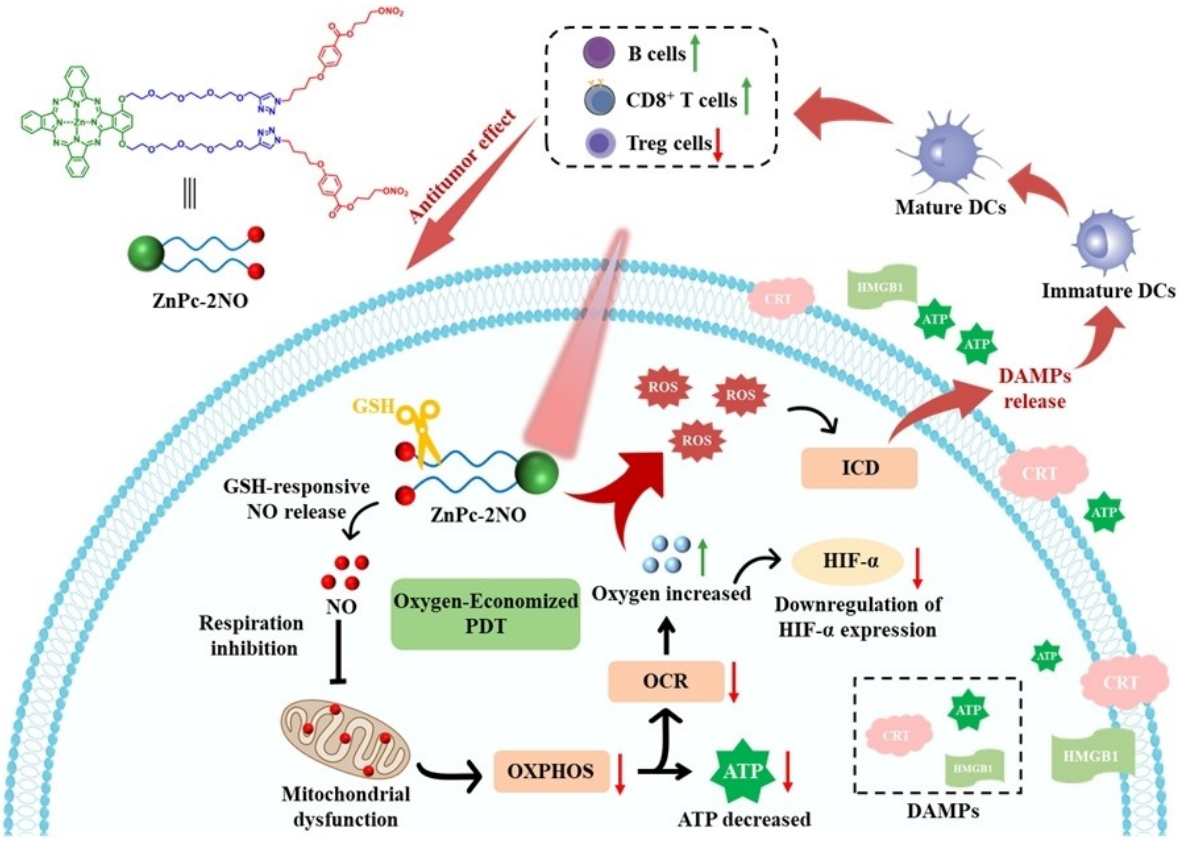

Figure 1. Mechanistic actions of the oxygen-economized PDT using **ZnPc-2NO** and the induced ICD. Upon internalization into cancer cells, **ZnPc-2NO** reacted with the enriched glutathione (GSH) to release NO, which interfered the normal functions of mitochondria to retard the oxidative phosphorylation (OXPHOS), thereby reducing the oxygen consumption rate (OCR) and adenosine triphosphate (ATP) generation, eventually reversing the tumor hypoxic status and downregulating the hypoxia-inducible factor 1α (HIF-1α) level for enhanced PDT. The photodynamic action could also induce the release of damage-associated molecular patterns (DAMPs), including calreticulin (CRT), ATP, and high-mobility group box-1 (HMGB1), triggering the maturation of dendritic cells (DCs) and elicitation of an antitumor immune response.

tumor immune response through **ZnPc-2NO**-induced oxygen-economized PDT was demonstrated through a series of in vitro and in vivo experiments as reported and discussed below.

Results and Discussion

Molecular Design, Synthesis, and Characterization

Among the different types of NO donors, organic nitrates were chosen because of their superior properties, including the rapid release of NO upon interaction with GSH, high safety profile of the by-products, and ease of preparation and chemical modification.[18] For the photosensitizing unit, a ZnPc was employed owing to the strong absorption in the far-red region, balanced fluorescence emission and ROS generation, and high stability of this class of functional dyes.[19] The target compounds were synthesized by a convergent approach outlined in Scheme 1. Substitution of methyl 4-(4-bromobutoxy)benzoate (**1**)[20] with NaN_3 in dimethyl sulfoxide (DMSO) gave **2**, which was then hydrolyzed to afford benzoic acid **3**. This compound was then coupled with NO donor **4**[21] or **5**[22] in the presence of 1-ethyl-3-(3-dimethylaminopropyl)carbodiimide (EDCI) and 4-dimethylaminopyridine (DMAP) to give the corresponding esters **6** and **7**, respectively. To prepare the ZnPc component, 2,3-dicyanohydroquinone (**8**) was treated with tosylate **9**[23] and K_2CO_3 in *N*,*N*-dimethylformamide (DMF) to give the dialkynyl phthalonitrile **10**, which underwent base-promoted mixed cyclization with an excess of phthalonitrile in the presence of $Zn(OAc)_2 \cdot 2H_2O$ to give ZnPc **11**, which could be isolated in 18% yield using column chromatography followed by size-exclusion chromatography. It is worth mentioning that although mixed cyclization of phthalonitriles generally gives a mixture of phthalocyanines, which may not be separated and purified readily, the use of unsubstituted phthalonitrile as one of the precursors and the introduction of one or two oligoethylene glycol chain(s) to another phthalonitrile precursor could facilitate these processes, leading to the isolation of the corresponding "3+1" phthalocyanines in reasonable yields.[24] With two alkynyl moieties, compound **11** could couple with two units of the azido NO donors **6** and **7** via copper-catalyzed azide-alkyne cycloaddition to give the target conjugates **ZnPc-2NO** and **ZnPc-4NO**, respectively. All the new compounds were characterized by various spectroscopic methods (Supporting Information).

Spectroscopic Properties and NO Release Kinetics

The electronic absorption and photophysical properties of **ZnPc-2NO** and **ZnPc-4NO** were first measured in DMF, using the non-NO-substituted analogue **11** for comparison. All the compounds exhibited typical electronic absorptions of zinc(II) phthalocyanines, displaying a B-band at 350 nm, a weak vibronic band at 610 nm, and a sharp and intense Q-band at 690 nm in the electronic absorption spectrum (Figure S1, Supporting Information). These spectral features

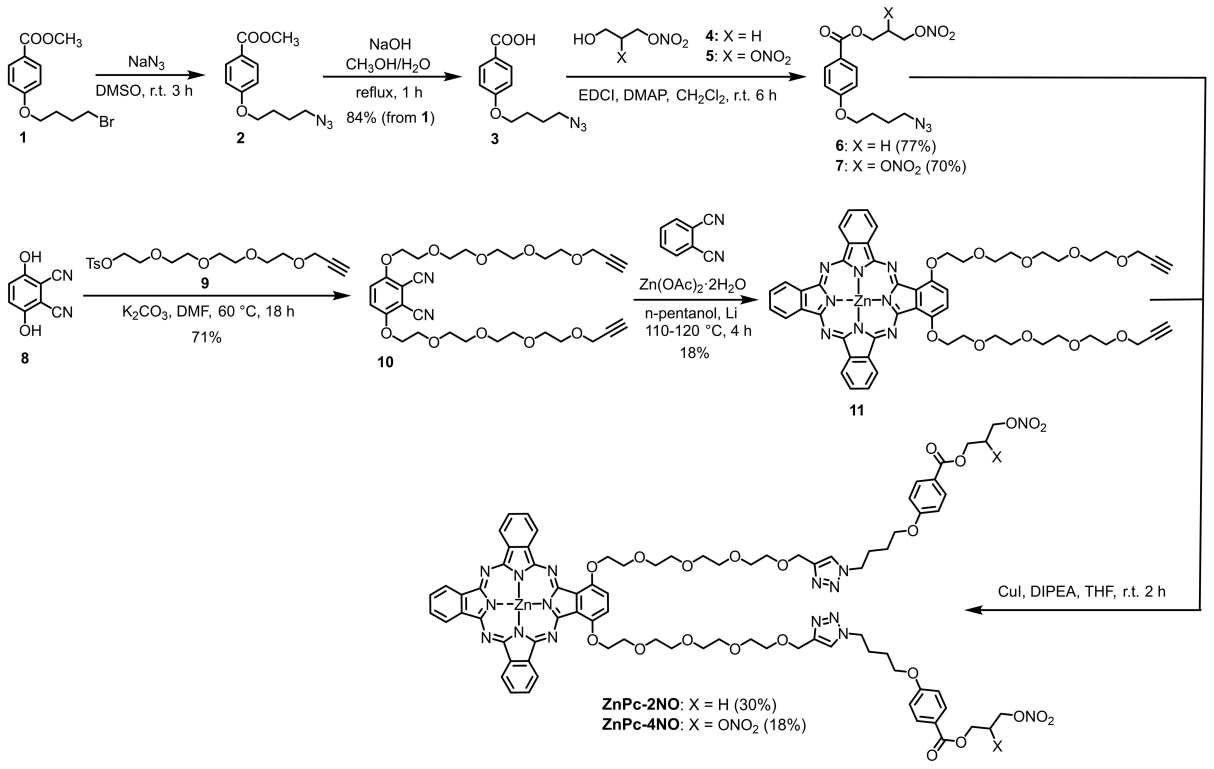

Scheme 1. Synthetic route of **ZnPc-2NO** and **ZnPc-4NO**.

indicated that the compounds are essentially non-aggregated under these conditions. Upon excitation at 610 nm, these compounds showed a strong fluorescence emission at 708–710 nm with a fluorescence quantum yield (Φ_F) of 0.15–0.16 relative to the unsubstituted ZnPc in DMF ($\Phi_F = 0.28$)[25] (Figure S2, Supporting Information, and Table 1). These spectral properties were also measured in phosphate-buffered saline (PBS) in the presence of DMF (10% v/v) and Tween 80 (1% v/v). The latter two substances were added to reduce the molecular aggregation of the phthalocyanines in aqueous media. Similar to the commonly used Cremophor EL, Tween 80 is also a polyethoxylated surfactant that can be used clinically for drug delivery.[26] All the compounds also exhibited a sharp and intense Q-band at 690–694 nm (Figure 2a) and a strong fluorescence emission at 711–714 nm (Figure 2b) in this aqueous medium. The virtually identical spectral features showed that the terminal NO-releasing units do not significantly perturb the electronic state of the ZnPc core in both of these media.

Table 1: Electronic absorption and photophysical data of **ZnPc-2NO**, **ZnPc-4NO**, **11**, and the unsubstituted ZnPc in DMF.

Compound	λ_{abs} (nm) (log ε)	λ_{em} (nm)[a]	Φ_F[b]	Φ_Δ[c]
ZnPc-2NO	350 (4.96), 610 (4.54), 690 (5.50)	710	0.16	0.60
ZnPc-4NO	350 (4.93), 610 (4.51), 690 (5.43)	708	0.16	0.61
11	350 (4.94), 610 (4.56), 690 (5.48)	708	0.15	0.64
ZnPc	350 (4.52), 610 (4.27), 670 (5.15)	685	0.28	0.56

[a] Excited at 610 nm. [b] Relative to ZnPc ($\Phi_F = 0.28$ in DMF). [c] Relative to ZnPc ($\Phi_\Delta = 0.56$ in DMF).

The singlet oxygen generation efficiency of these compounds was then examined in DMF using 1,3-diphenylisobenzofuran (DPBF) as the singlet oxygen scavenger. Upon light irradiation, all of them could generate singlet oxygen efficiently as reflected by the rapid decrease in the absorbance at the DPBF's absorption at 416 nm (Figure 2c). The singlet oxygen quantum yields (Φ_Δ) were determined to be 0.60–0.64 relative to the unsubstituted ZnPc ($\Phi_\Delta = 0.56$).[25] Table 1 compiles all these spectroscopic and photo-

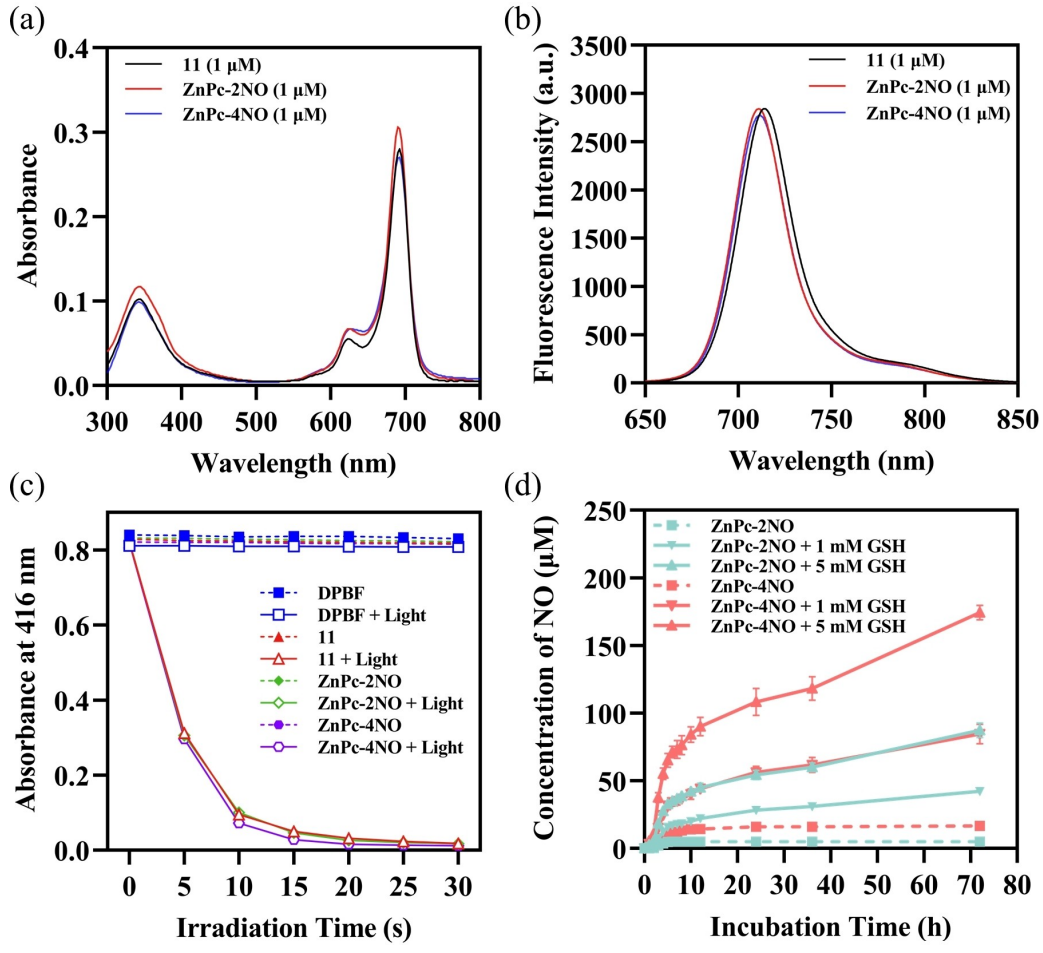

Figure 2. Electronic absorption, photophysical, and NO-releasing properties. (a) Electronic absorption and (b) fluorescence ($\lambda_{ex} = 610$ nm) spectra of **ZnPc-2NO**, **ZnPc-4NO**, and **11** (1 μM) in PBS with 10% (v/v) DMF and 1% (v/v) Tween 80. (c) Comparison of the rates of decay of DPBF (initial concentration = 30 μM) with or without the presence of **ZnPc-2NO**, **ZnPc-4NO**, or **11** (1 μM) and light irradiation ($\lambda > 610$ nm) in DMF, as indicated by the decrease of absorbance at 416 nm. (d) Cumulative release of NO from **ZnPc-2NO** and **ZnPc-4NO** (250 μM) with or without the presence of GSH (1 or 5 mM) in DMF over a period of time, as determined by a colorimetric Griess assay.

physical data recorded in DMF, including those of the unsubstituted ZnPc for comparison.

The GSH-responsive release of NO from **ZnPc-2NO** and **ZnPc-4NO** was then monitored using a Griess assay.[27] In this assay, the released NO is first oxidized rapidly to nitrite (NO_2^-), which is a stable and non-volatile metabolite of NO, and this species further reacts with sulphanilamide (Griess reagent I) and then *N*-(1-naphthyl)ethylenediamine (Griess reagent II) to form a diazonium species with an absorption at 540 nm. The NO concentration can be determined by measuring the absorbance at this position with reference to a standard curve of $NaNO_2$ aqueous solution. To perform this study, solutions of **ZnPc-2NO** and **ZnPc-4NO** in DMF (250 μM) with or without GSH (1 or 5 mM) were prepared. At different time points, an aliquot of the mixtures (50 μL) was withdrawn, and the amount of NO released was determined by this colorimetric NO assay. As shown in Figure 2d, while both conjugates could not generate NO in the absence of GSH, the addition of GSH could promote the release of NO, and with additional nitrate substituents, **ZnPc-4NO** could generate more NO as expected.

In Vitro Studies

The cellular uptake of **11**, **ZnPc-2NO**, and **ZnPc-4NO** was then studied against HT29 human colorectal adenocarcinoma cells using confocal microscopy and flow cytometry. It was found that all of them could be internalized readily, exhibiting a strong fluorescence signal inside the cells, and the quantified intracellular fluorescence intensities were not significantly different for the three compounds and for the four incubation times used (2, 4, 6, and 12 h) (Figure S3, Supporting Information).

The release of NO from **ZnPc-2NO** and **ZnPc-4NO** inside the cells was then studied using 4-amino-5-methylamino-2,7-difluorofluorescein diacetate (DAF-FM-DA) as the probe,[28] which is converted into 4-amino-5-methylamino-2,7-difluorofluorescein (DAF-FM) upon hydrolysis by the intracellular esterase, and then it reacts with NO to form a highly fluorescent benzotriazole fluorescein derivative (DAF-FM-T). Briefly, HT29 cells were incubated in the culture medium with or without **11**, **ZnPc-2NO**, or **ZnPc-4NO** (1 or 2 μM) for different periods of time (2, 6, or 12 h), followed by the incubation with DAF-FM-DA (5 μM) for 30 min. The cellular images and the intracellular fluorescence intensities were then determined and compared. As shown in Figure 3a, the signal of DAF-FM-T could clearly be seen for the cells being treated with **ZnPc-2NO** or **ZnPc-4NO**, but not for those being incubated in the culture medium with or without **11**. The intensity was increased with the incubation time, showing that NO was released from these cells in a time-dependent manner. The mean intracellular fluorescence intensity for **ZnPc-2NO** (at 2 μM) was very similar to that for **ZnPc-4NO** (at 1 μM), which has 2-fold NO-releasing units compared with the former (Figure 3b). Surprisingly, when 2 μM of **ZnPc-4NO** was used, the intensity was only marginally increased, which was not consistent with the results in solution study (Figure 2d). It might be attributed to the insufficient GSH inside the cells to trigger the release of NO or the limited sensitivity of the NO probe.

To reveal the situation, we measured the intracellular GSH levels of HT29 cells after incubation in the neat culture medium or with **11**, **ZnPc-2NO**, or **ZnPc-4NO** (1 or 2 μM) for 12 h, using ThiolTracker™ Violet as a GSH probe. It was found that while the level was virtually unchanged upon incubation with **11**, it was significantly reduced when the cells were treated with **ZnPc-2NO** or **ZnPc-4NO** (Figure S4, Supporting Information), showing that the intracellular GSH was consumed. The similar GSH levels for all these conditions, including the use of 2 μM of **ZnPc-4NO**, showed that the similar intracellular NO concentrations observed (Figure 3b) should be due to the limited amount of GSH inside the cells.

The effect of these conjugates on the cellular respiration was also investigated by monitoring the relative oxygen content in the medium containing the cancer cells over a period of time. In this study, HT29 cells were incubated in the culture medium with or without **11**, **ZnPc-2NO**, or **ZnPc-4NO** (1 or 2 μM) for 8 h, during which the medium was sealed with liquid paraffin to exclude external oxygen supply. The dissolved oxygen content in the medium was measured by an oxygen meter at different time points over a further period of 30 min. As shown in Figure 3c, the oxygen content was largely decreased (to ca. 60 % in 30 min) in the medium containing the cells with or without the treatment with **11**, which could be attributed to regular cellular respiration. Upon treatment with **ZnPc-2NO** or **ZnPc-4NO**, the oxygen content was significantly higher and decreased in less than 20 % in 30 min. Considering that ATP is the main product of cellular respiration, the intracellular ATP content was also determined after the aforementioned treatments using a luminescent ATP detection kit. As shown in Figure 3d, the ATP content was reduced to about 50 % after the treatment with **ZnPc-2NO** (2 μM) or **ZnPc-4NO** (1 μM) for 12 h compared with those in the cells being incubated in the medium with or without **11**. The reduction was further enhanced when the concentration of **ZnPc-4NO** was increased to 2 μM. All these results suggested that the cellular respiration of these cancer cells could be inhibited by these conjugates due to the released NO.

In addition, the influence of the conjugates on the mitochondrial membrane potential ($\Delta\Psi_m$) was also investigated using 5,5′,6,6′-tetrachloro-1,1′,3,3′-tetraethylbenzimidazolo-carbocyanine iodide (JC-1) as an indicator, which exhibits potential-dependent accumulation in mitochondria. At high $\Delta\Psi_m$, JC-1 forms aggregates and exhibits red fluorescence at 590 nm, while it exists as a monomer at low $\Delta\Psi_m$ and emits green fluorescence at 525 nm. The decrease in the ratio of red to green fluorescence intensity indicates mitochondrial depolarization, which is a feature of mitochondrial dysfunction. To perform this study, HT29 cells were incubated in the culture medium with or without **11**, **ZnPc-2NO**, or **ZnPc-4NO** (1 or 2 μM) for 12 h, followed by staining with JC-1 (10 $\mu g\,mL^{-1}$) for 30 min. It was found that the mitochondrial membrane was depolarized in the cells

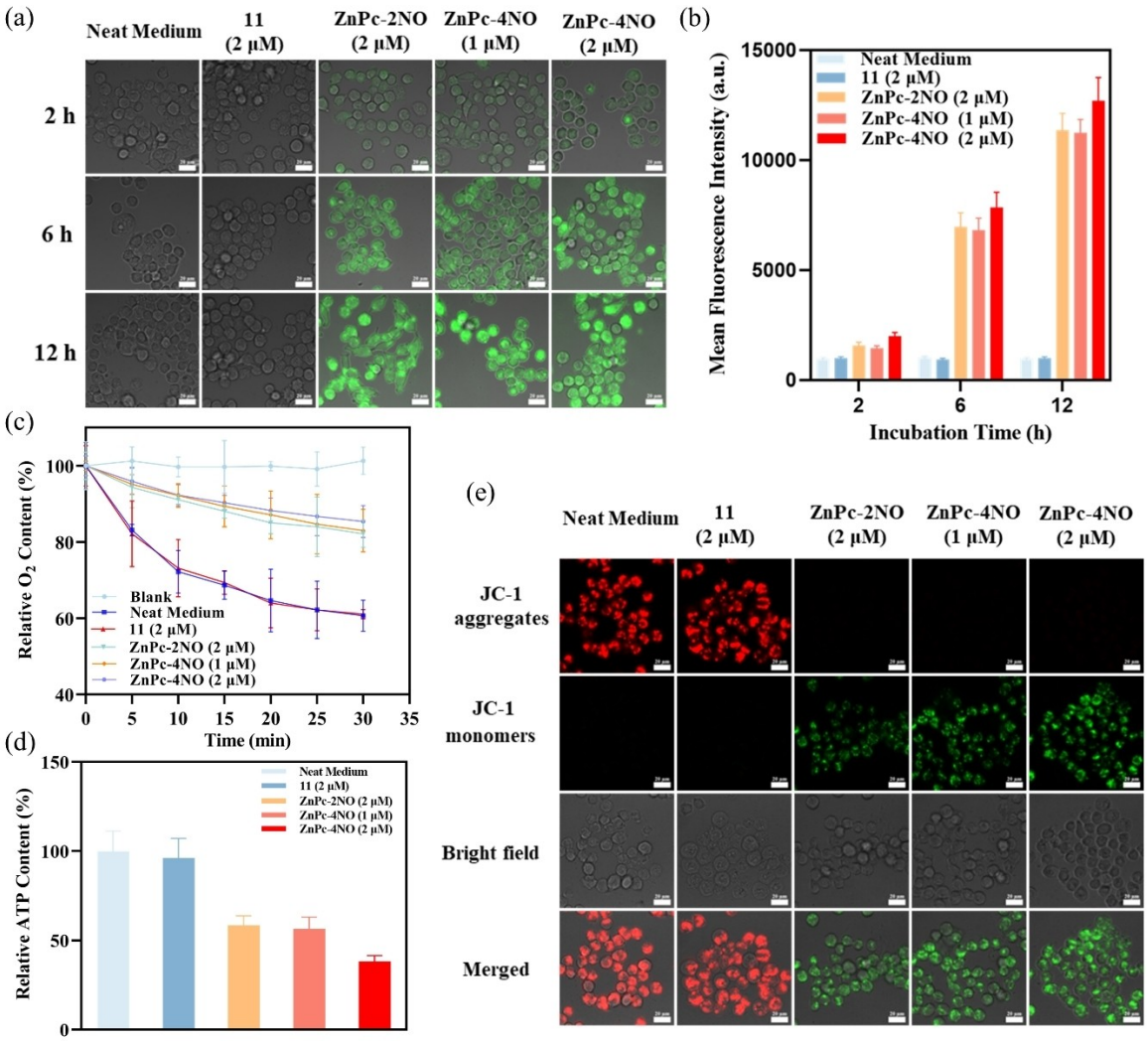

Figure 3. Intracellular release of NO and its effects on HT29 cells. (a) Fluorescence images of HT29 cells after being incubated in the culture medium with or without **11**, **ZnPc-2NO**, or **ZnPc-4NO** (1 or 2 μM) for different periods of time, followed by incubation with DAF-FM-DA (5 μM) for 30 min (λ_{ex} = 488 nm, λ_{em} = 495–600 nm). The NO generation efficiency is reflected by the intracellular fluorescence intensity of DAF-FM-T generated. (b) Mean fluorescence intensities of DAF-FM-T in HT29 cells after the above treatments as determined by flow cytometry (λ_{ex} = 488 nm, λ_{em} = 505–545 nm). (c) Change in dissolved oxygen content in the culture medium containing HT29 cells after being incubated in the culture medium with or without **11**, **ZnPc-2NO**, or **ZnPc-4NO** (1 or 2 μM) for 8 h over a period of 30 min. (d) Relative ATP content of HT29 cells after being incubated in the culture medium with or without **11**, **ZnPc-2NO**, or **ZnPc-4NO** (1 or 2 μM) for 12 h. (e) Analysis of $\Delta\Psi_m$ on HT29 cells upon incubation in the culture medium with or without **11**, **ZnPc-2NO**, or **ZnPc-4NO** (1 or 2 μM) for 12 h, followed by staining with JC-1 (10 μg mL^{-1}) for 30 min (red fluorescence: λ_{ex} = 561 nm, λ_{em} = 570–680 nm; green fluorescence: λ_{ex} = 488 nm, λ_{em} = 495–550 nm). Data are expressed as the mean ± standard deviation (SD) of three independent experiments, and scale bar = 20 μm in the relevant figures.

being treated with **ZnPc-2NO** or **ZnPc-4NO**, while minimal changes were observed for the **11**-treated cells (Figure 3e), indicating that the released NO also induced mitochondrial dysfunction.

The hypoxic status of the cells after these treatments under a hypoxic condition (with 1 % oxygen) was further examined using the ROS-ID fluorogenic hypoxia probe, in which the nitro group is converted to hydroxylamine and an amine by the nitroreductase inside the hypoxic cells to release a fluorophore. As shown in Figure 4a, a strong fluorescence signal was observed for HT29 cells being cultured in a neat medium or in the presence of **11**. For the cells being incubated with **ZnPc-2NO** or **ZnPc-4NO**, the intracellular fluorescence was significantly weaker and comparable with that for the cells being cultured under a normoxic (with 21 % oxygen) condition. The fluorescence intensities under these conditions were also quantified by flow cytometry. It was found that the intensity was reduced by ca. 60 % after the treatment with **ZnPc-2NO** or **ZnPc-4NO**, and increasing the concentration of **ZnPc-4NO** did not lead to further reduction of the intensity (Figure 4b). This again indicated that even though **ZnPc-4NO** could release more NO in solution, it was not the case inside the cells, and **ZnPc-2NO** was already an effective NO-releasing photosensitizer.

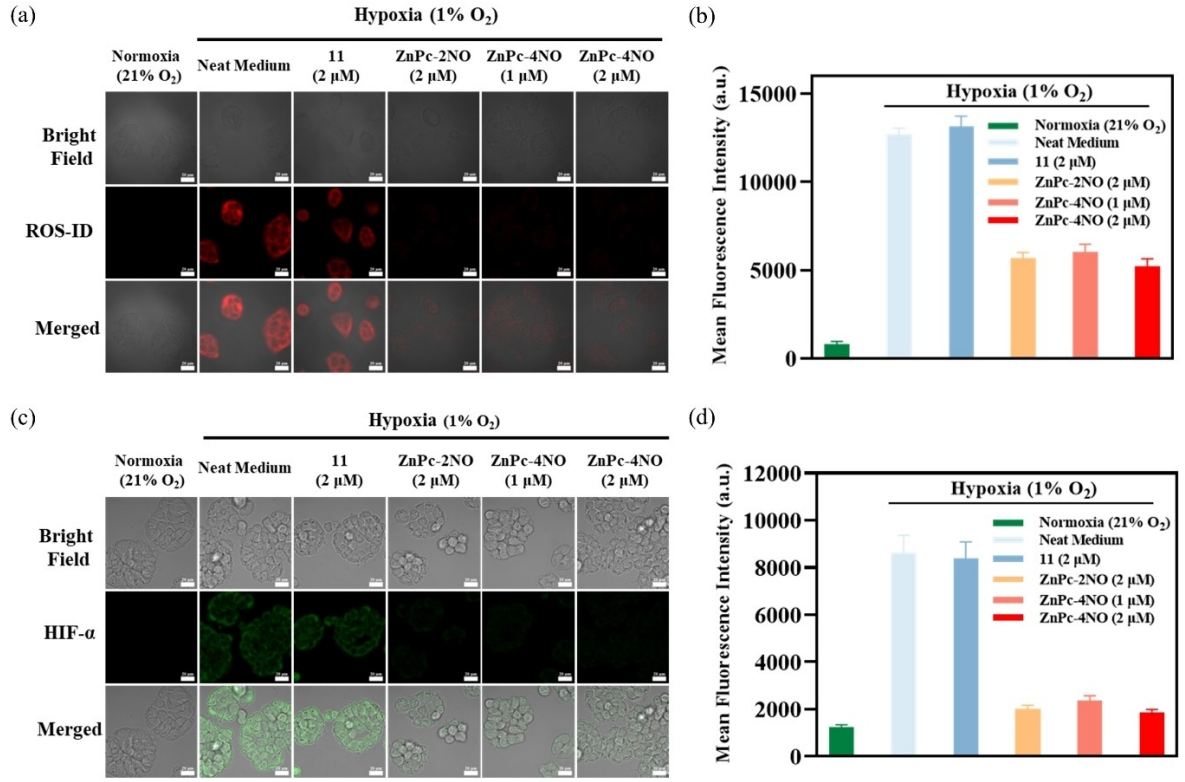

Figure 4. Effects on the hypoxic status and HIF-1α level in HT29 cells. (a) Hypoxic status of HT29 cells as reflected by the intracellular fluorescence intensity of ROS-ID. The cells were incubated in the culture medium under a normoxic (21 % O_2) or hypoxic (1 % O_2) condition or in the presence of **11**, **ZnPc-2NO**, or **ZnPc-4NO** (1 or 2 μM) under a hypoxic condition for 12 h, followed by incubation with ROS-ID (5 μM) for 1 h (λ_{ex} = 561 nm, λ_{em} = 570–680 nm). (b) Mean fluorescence intensities of ROS-ID in HT29 cells after the above treatments as determined by flow cytometry (λ_{ex} = 561 nm, λ_{em} = 564–606 nm). (c) HIF-1α immunostaining for HT29 cells after incubation in the culture medium under a normoxic or hypoxic condition or in the presence of **11**, **ZnPc-2NO**, or **ZnPc-4NO** (1 or 2 μM) under a hypoxic condition for 12 h (λ_{ex} = 488 nm, λ_{em} = 493–565 nm). (d) Mean fluorescence intensities of HIF-1α immunostaining in HT29 cells after the above treatments as determined by flow cytometry (λ_{ex} = 488 nm, λ_{em} = 493–565 nm). Data are expressed as the mean ± SD of three independent experiments, and scale bar = 20 μm in the relevant figures.

As HIF-1α is usually upregulated in tumors and plays an important role in tumor metastasis and angiogenesis,[5] its expression in the HT29 cells being treated as described above was also examined using an immunostaining method. The trend of the HIF-1α level, as reflected by the relative intracellular fluorescence intensity (Figure 4c and 4d), was in good agreement with that of the hypoxic status of the cells (Figure 4a and 4b), confirming that these NO-releasing compounds could mitigate hypoxia and downregulate HIF-1α by inhibiting the cellular respiration.

NO-inhibited cellular respiration was believed to conserve more intracellular oxygen for the photodynamic action, which might overcome the problem of tumor hypoxia. To validate this hypothesis, ROS generation inside the HT29 cells after the aforementioned treatments was examined under both normoxic and hypoxic conditions, using 2′,7′-dichlorodihydrofluorescein diacetate (H_2DCFDA) as a probe, which would be deacetylated by the esterase and then oxidized by the ROS inside the cells to give highly fluorescent 2',7'-dichlorofluorescein (DCF). It was found that all three photosensitizers could generate ROS upon light irradiation under a normoxic condition, as shown by the strong fluorescence of DCF (Figure 5a). In contrast, only **ZnPc-2NO** and **ZnPc-4NO** could significantly produce ROS inside the cells under hypoxia, whereas ROS generation was largely inhibited in the cells being incubated with **11** (Figure 5b). In **11**-treated HT29 cells, the quantified intracellular fluorescence intensity of DCF was only about 30 % of that for the **ZnPc-2NO** and **ZnPc-4NO**-treated counterparts (Figure 5c).

The dark and photo-cytotoxicities of **ZnPc-2NO** and **ZnPc-4NO** were further investigated under both normoxic and hypoxic conditions and compared with those of **11**. In the absence of light irradiation, all the photosensitizers were found to be essentially non-cytotoxic up to a concentration of 1–2 μM. At 4 μM, **ZnPc-4NO** became slightly cytotoxic, reducing the cell viability by ca. 30 %. The results were similar under normoxic (Figure 5d) and hypoxic (Figure 5e) conditions. Upon light irradiation ($\lambda > 610$ nm, 18 mW cm^{-2}, 1.08 J cm^{-2}), all the photosensitizers showed comparable and concentration-dependent cytotoxicity under normoxia (Figure 5f). Interestingly, while the photocytotoxicity of **11** was significantly reduced under hypoxia, **ZnPc-2NO** and **ZnPc-4NO** remained highly potent and could kill almost all the cells at a drug dose of 4 μM (Figure 5g). The overall results showed that both **ZnPc-2NO** and **ZnPc-4NO** could alleviate

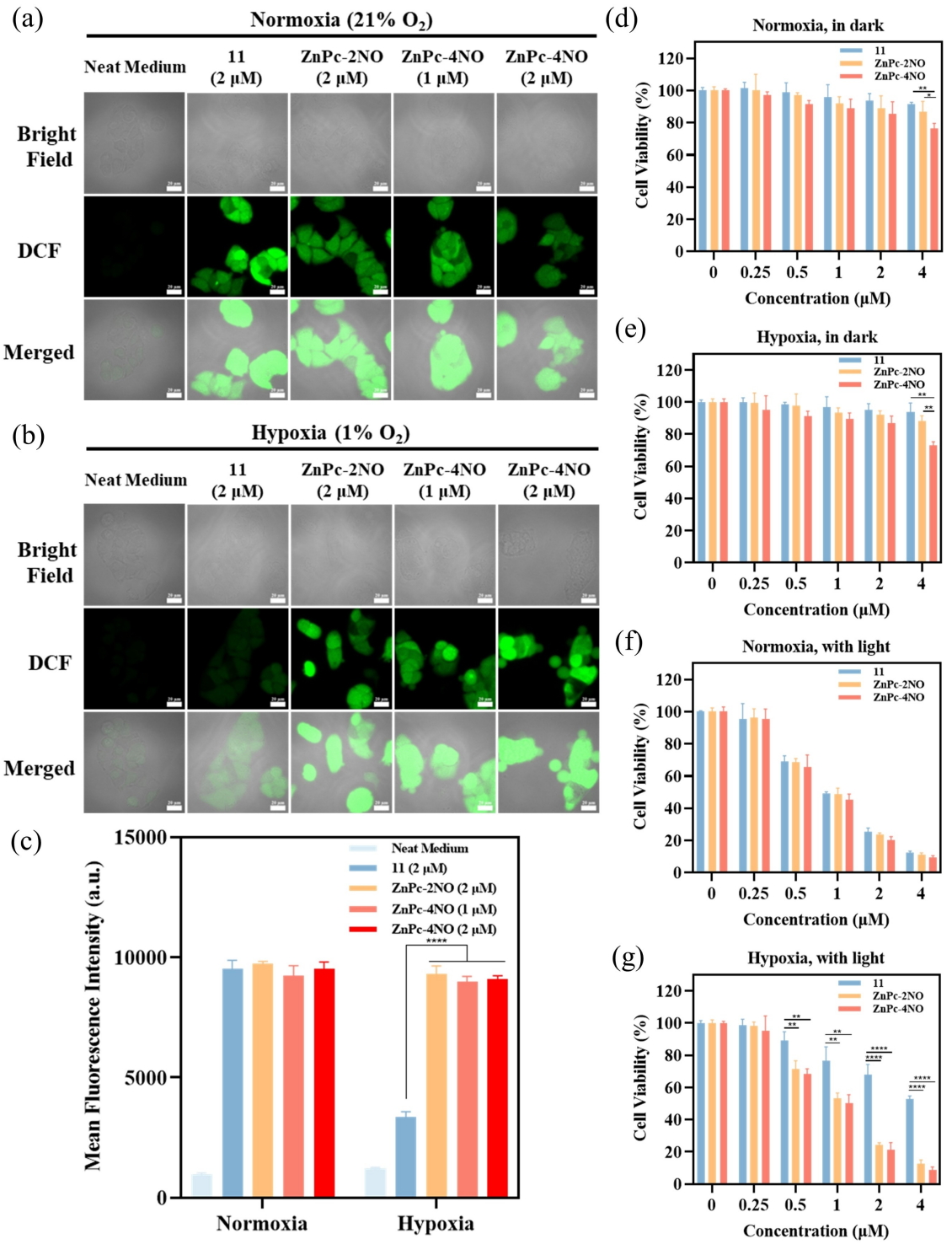

Figure 5. Intracellular ROS generation and cytotoxicity against HT29 cells under normoxia and hypoxia. Bright field, fluorescence, and the merged images of HT29 cells after incubation in the culture medium with or without **11**, **ZnPc-2NO**, or **ZnPc-4NO** (1 or 2 μM) under a (a) normoxic or (b) hypoxic condition for 12 h, followed by incubation with H_2DCFDA (10 μM) for 30 min and light irradiation ($\lambda > 610$ nm, fluence rate = 18 mW cm^{-2}) for 1 min ($\lambda_{ex} = 488$ nm, $\lambda_{em} = 505–545$ nm). Scale bar = 20 μm. (c) Quantified fluorescence intensities of the cells being treated as described above determined by flow cytometry. Data are expressed as the mean ± SD of three independent experiments. (d, e) Dark and (f, g) photo-cytotoxicities of **11**, **ZnPc-2NO**, and **ZnPc-4NO** against HT29 cells under (d, f) normoxia or (e, g) hypoxia ($\lambda > 610$ nm, 18 mW cm^{-2}, 1.08 J cm^{-2}). Data are expressed as the mean ± standard error of the mean (SEM) of three independent experiments, each performed in quadruplicate. *$P < 0.05$, **$P < 0.01$, ***$P < 0.001$, ****$P < 0.0001$.

the hypoxic status of the cells via inhibition of cellular respiration, thereby sparing more oxygen for effective photodynamic elimination of cancer cells even under hypoxia.

All the aforementioned in vitro studies were also performed using A549 human lung carcinoma cells. Both cell lines are widely used in in vitro studies due to their unique characteristics. HT29 cells are well known for their aggressive and metastatic nature, which is a characteristic feature of colorectal adenocarcinoma.[29] They are particularly sensitive to chemotherapeutic drugs such as oxaliplatin, a standard treatment for colorectal cancer. However, under hypoxic conditions, HT29 cells exhibit resistance to platinum-based drugs.[30] This response makes them an excellent cell-line model for studying drug resistance, which is a significant challenge in colorectal cancer treatment. On the other hand, A549 cells maintain many characteristics of normal lung epithelium. They are enriched in proteins associated with cellular respiration, ubiquitination, apoptosis, and response to drug/hypoxia/oxidative stress.[31] These cells also exhibit a relatively high invasion ability,[32] making them a suitable in vitro model for studying the effects of drugs on cell proliferation, invasion, and metastasis. Therefore, these two cell lines were chosen for the in vitro studies in order to provide a broader context for understanding the therapeutic potential and mechanism of the photosensitizers. The results for A549 cells were found to be very similar to those for HT29 cells (Figure S5–S14, Supporting Information), showing that the in vitro properties of **ZnPc-2NO** and **ZnPc-4NO** were not cell selective.

To provide further evidence, human embryonic kidney 293 (HEK-293) cells, which are one of the most widely used standards for normal human cells,[33] were also used to compare cellular uptake and cytotoxicity. As shown in Figure S15 (Supporting Information), the intracellular fluorescence intensities of **11**, **ZnPc-2NO**, and **ZnPc-4NO** were not significantly different upon incubation for 2, 4, 6, or 12 h. Under a normoxic or hypoxic condition, the trends of dark and photo-cytotoxicities were also very similar to those for HT29 and A549 cells (Figure S16, Supporting Information). Table 2 summarizes the half-maximal inhibitory concentrations (IC_{50} values) of all these photosensitizers against the three cell lines under normoxic and hypoxic conditions. It can be seen that the values for **ZnPc-2NO** and **ZnPc-4NO** were similar for each of these cell lines. In addition, while the photocytotoxicity of **11** was similar to that of **ZnPc-2NO** and **ZnPc-4NO** under normoxia, this non-NO-substituted analogue was significantly less photocytotoxic under hypoxia, and its IC_{50} values could not be determined.

Study of Immunogenic Cell Death

ICD is a cell death mechanism characterized by the release of various DAMPs that trigger an immune response. Previous studies have demonstrated that PDT can trigger an ICD-mediated antitumor immune response by inducing the release of tumor-associated DAMPs, such as CRT translocated from the endoplasmic reticulum to the cell surface, HMGB1 released from the nucleus, and ATP from the mitochondria, thus stimulating the maturation of DCs.[34] In fact, even with a sub-lethal light dose, the photodynamic process can alter the cellular, stromal, and/or vascular microenvironment, making it more susceptible to subsequent therapies, such as chemotherapy, radiation therapy, and immunotherapy. This process termed photodynamic priming has emerged as a promising strategy for promoting therapeutic benefits and overcoming treatment resistance.[35] It can modulate the tumor microenvironment, enhance the immunogenicity of tumors, and improve the outcome of immunotherapy by inducing ICD.[36]

To investigate the potential of these NO-releasing photosensitizers to induce ICD through PDT, **ZnPc-2NO** was first selected for this study against HT29 cells. We first examined the level of cell surface CRT and the extracellular levels of HMGB1 and ATP in the cell culture medium according to the protocols outlined in Figure 6a. We observed strong CRT immunofluorescence on the cells being treated with **ZnPc-2NO** and light irradiation, while the signal for the cells without being incubated with **ZnPc-2NO** was negligible (Figure 6b). Using a colorimetric enzyme-linked immunosorbent assay (ELISA) and a luminescent ATP detection assay kit, it was found that the photodynamic action of **ZnPc-2NO** could significantly enhance the release of HMGB1 and ATP from the cells, as compared to the non-**ZnPc-2NO**-treated or non-irradiated controls (Figure 6c and 6d). Together, these results demonstrated that PDT sensitized by **ZnPc-2NO** could induce ICD and trigger the release of these DAMPs in HT29 cells.

The study was then extended to **ZnPc-4NO** and **11** to reveal whether this effect is dependent on the substituents. It was found that these DAMPs could also be released upon the action of these photosensitizers in the presence of light

Table 2: IC_{50} values of **11**, **ZnPc-2NO**, and **ZnPc-4NO** against HT29, A549, and HEK-293 cells under normoxia and hypoxia with light irradiation ($\lambda > 610$ nm, 18 mW cm^{-2}, 1.08 J cm^{-2}).

Compound	IC_{50} (μM)					
	Normoxia			Hypoxia		
	HT29	A549	HEK-293	HT29	A549	HEK-293
11	1.61 ± 0.06	2.23 ± 0.05	1.36 ± 0.11	–[a]	–[a]	–[a]
ZnPc-2NO	1.52 ± 0.05	1.92 ± 0.03	0.99 ± 0.09	1.59 ± 0.05	2.03 ± 0.11	1.92 ± 0.24
ZnPc-4NO	1.39 ± 0.02	1.73 ± 0.08	0.85 ± 0.07	1.52 ± 0.09	1.87 ± 0.10	1.66 ± 0.21

[a] The value could not be determined up to 4 μM.

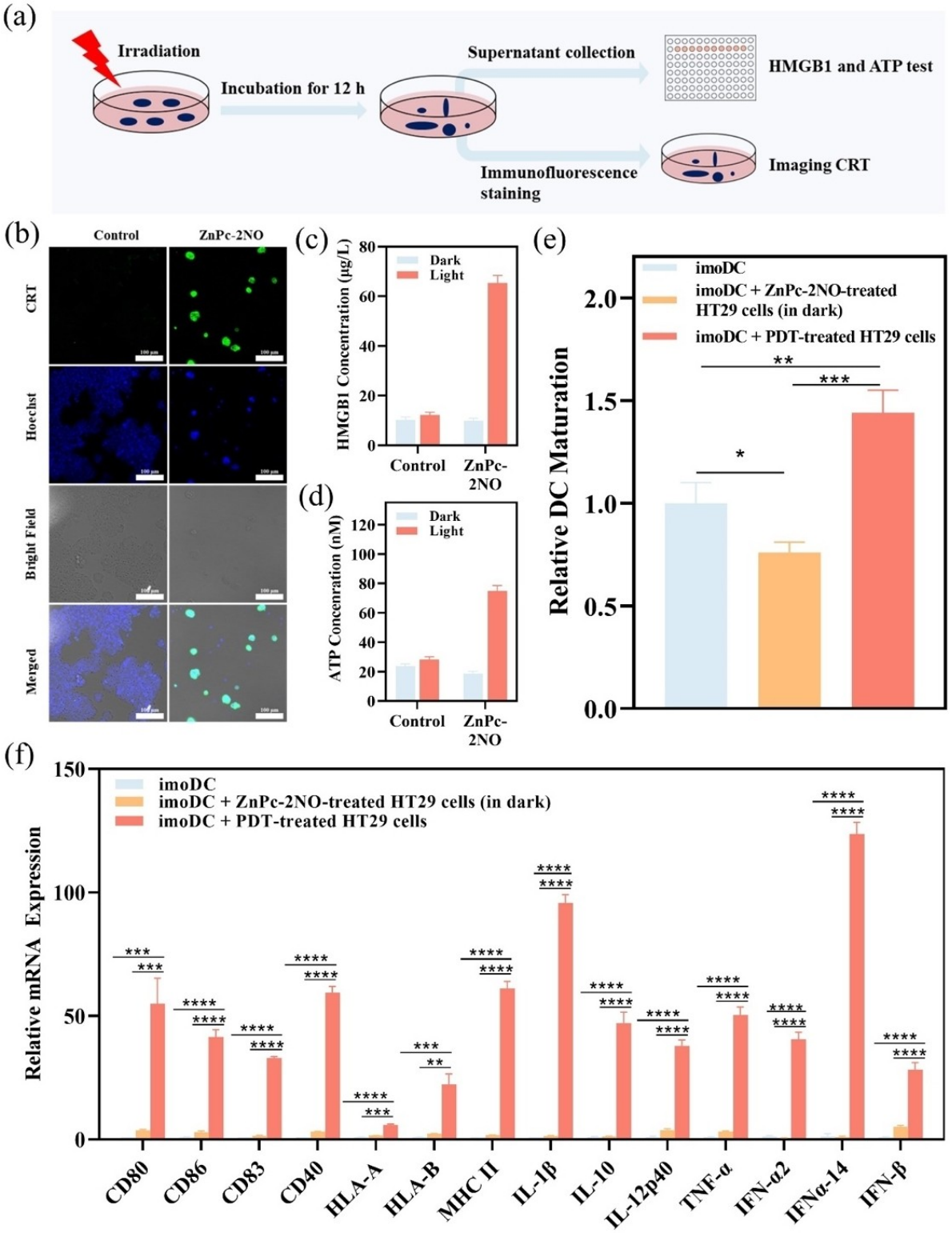

Figure 6. ICD induced by **ZnPc-2NO**-mediated PDT against HT29 cells. (a) Illustration of CRT, HMGB1, and ATP tests. (b) Confocal microscopic images of HT29 cells with CRT staining ($\lambda_{ex}=488$ nm, $\lambda_{em}=493$–550 nm; for Hoechst: $\lambda_{ex}=405$ nm, $\lambda_{em}=460$–490 nm) after the treatment with **ZnPc-2NO** (2 μM) for 12 h followed by light irradiation ($\lambda>610$ nm, 18 mW cm^{-2}) for 1 min. The light-irradiated non-**ZnPc-2NO**-treated HT29 cells were used as control. Scale bar = 100 μm. The extracellular (c) HMGB1 and (d) ATP levels of HT29 cells after the incubation in the medium with or without **ZnPc-2NO** (2 μM) for 12 h and with or without the subsequent light treatment as described above determined by a HMGB1 ELISA kit and an ATP bioluminescence kit, respectively. (e) Relative maturation of DCs induced by the **ZnPc-2NO**-treated HT29 cells with or without light irradiation using CD80 and CD86 as markers. (f) Relative mRNA levels of various markers of mature DCs after the aforementioned treatments. Data have been normalized to the 'Blank' values and analyzed by the 2-ΔΔCt method using β-actin as a reference gene. *$P<0.05$, **$P<0.01$, ***$P<0.001$, ****$P<0.0001$.

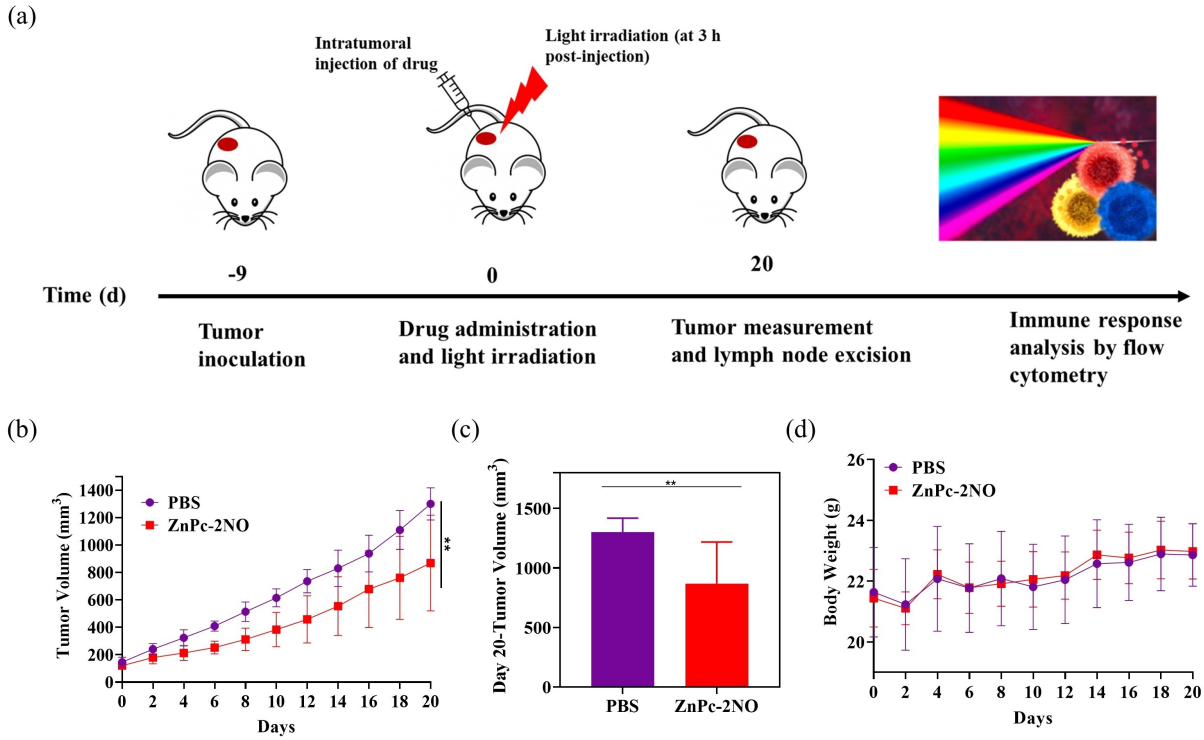

Figure 7. In vivo antitumor effect of **ZnPc-2NO**. (a) Schematic illustration of the experimental design to examine the antitumor immune response triggered by **ZnPc-2NO**-mediated PDT. (b) Tumor growth curves for the **ZnPc-2NO**- and PBS-treated mice after laser irradiation. (c) Comparison of the tumor volumes of these two groups of mice on day 20. (d) Change in the body weight of these two groups of mice over a period of 20 days. $^{**}P < 0.01$.

irradiation, but not in the dark (Figure S17, Supporting Information). The extent of CRT translocation to the cell membrane and the secreted level of HMGB1 triggered by the photodynamic effect of these two photosensitizers were comparable with those for **ZnPc-2NO**. However, the ATP concentration was significantly higher in the **11**-treated cell supernatant, which could be attributed to the reduced ATP levels in **ZnPc-2NO** and **ZnPc-4NO**-treated HT29 cells as a result of the NO-mediated inhibition of ATP production (Figure 3d). These results suggested that all these zinc(II) phthalocyanines could trigger ICD upon light irradiation regardless of the presence and number of the NO donor. Nevertheless, the unique NO-releasing property of **ZnPc-2NO** and **ZnPc-4NO** could effectively retard cellular respiration and relieve the hypoxic status of cancer cells, thereby overcoming the oxygen-dependent nature of PDT. As the intracellular NO-releasing ability of the two photosensitizers was comparable as mentioned above, **ZnPc-2NO** was chosen for further biological evaluation.

To evaluate the ability of **ZnPc-2NO** to induce ICD through PDT for the maturation of DCs, immature monocyte-derived DCs (imoDCs) were co-cultured with the PDT-treated HT29 cells for 24 h, and the proportion of $CD80^+$ and $CD86^+$ mature DCs was then measured by flow cytometry. As shown in Figure 6e, the proportion of mature DCs increased significantly after co-culturing with the PDT-treated HT29 cells, as compared to imoDCs without co-culturing and those after co-culturing with the **ZnPc-2NO**-treated HT29 cells but without light irradiation, indicating that the PDT-treated HT29 cells could stimulate the maturation of DCs. We also assessed the levels of other activation markers of DCs by quantitative polymerase chain reaction (qPCR) and observed an enhancement in the mRNA expression of CD80, CD86, CD83, CD40, HLA-A, HLA-B, and MHC II upon co-culturing with the PDT-treated cells (Figure 6f). These results strongly suggested that the PDT treatment of HT29 cells using **ZnPc-2NO** could promote the maturation of DCs, which is essential for the activation of antitumor immunity. We then assessed the production of various inflammatory cytokines when the DCs were co-cultured with the PDT-treated HT29 cells. Compared to the two controls mentioned above, these DCs expressed significantly higher levels of interleukin 1β (IL-1β), interleukin 10 (IL-10), interleukin 12 (IL-12p40), and tumor necrosis factor α (TNF-α) as measured by qPCR. These cytokines are known to promote inflammation and activate the adaptive immunity. The mRNA expression of Type I interferons (IFNs), including IFN-α2, IFN-α14, and IFN-β, which have potent anticancer effects, also significantly increased in the DCs after co-culturing with the PDT treated-HT29 cells. These results clearly indicated that the **ZnPc-2NO**-photosensitized cell death was immunogenic and evoked a robust DC-mediated response for enhanced antitumor efficacy.

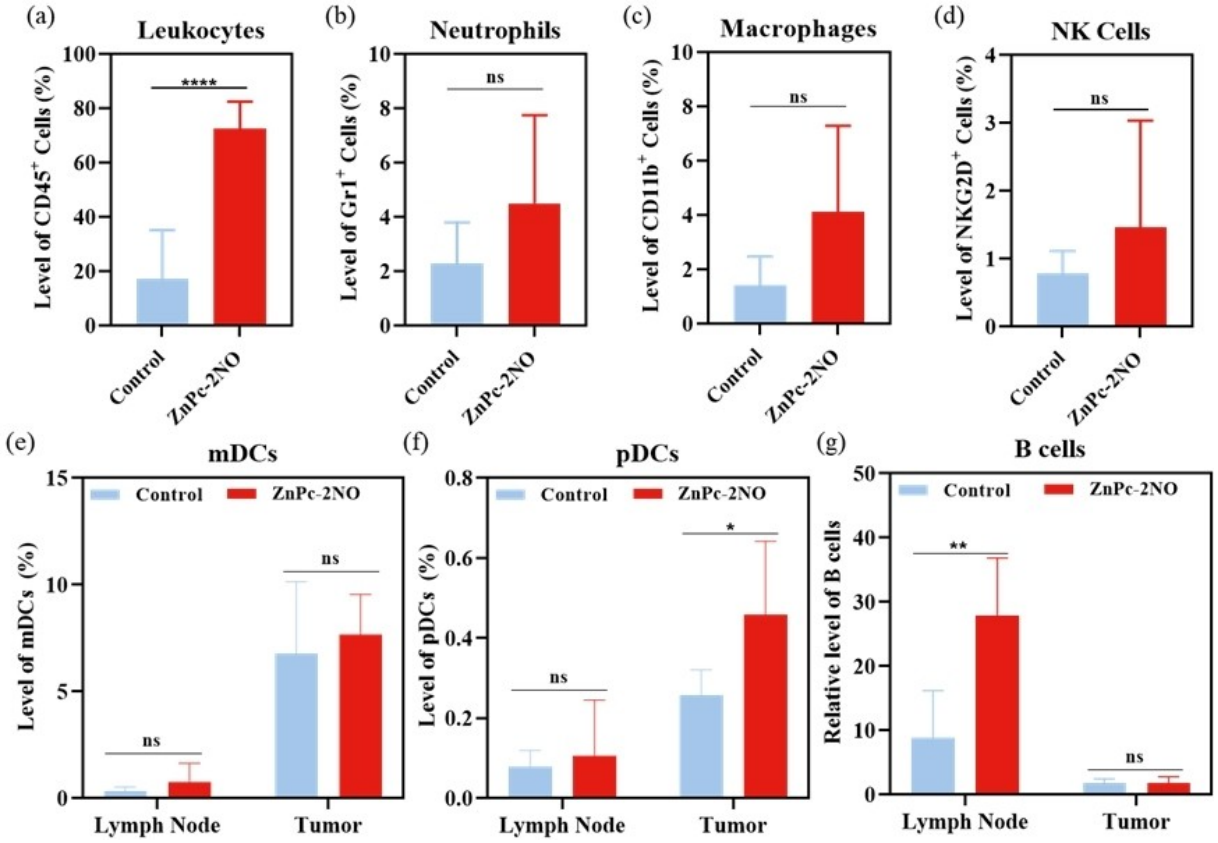

Figure 8. Population of innate immune cells in the lymph nodes on day 20, including (a) leukocytes (b) neutrophils (c) macrophages, and (d) NK cells. The relative levels of (e) mDCs, (f) pDCs, and (g) B cells in the lymph nodes and tumor site on day 20. n.s. not significant, *$P < 0.05$, **$P < 0.01$, ****$P < 0.0001$.

In Vivo Studies

To assess the in vivo antitumor efficacy of **ZnPc-2NO**, a breast-tumor animal model was established by inoculating 4T1 cells into the mammary fat pad of female Balb/c mice. The mice were randomly distributed into two groups when the tumor volume reached ca. 50 mm^3. Light irradiation (675 nm laser at 0.1 $W\,cm^{-2}$ for 5 min) was applied on the tumor at 3 h after the intratumoral injection of PBS or **ZnPc-2NO** in PBS with 1 % (v/v) DMSO and 0.1 % (v/v) Tween 80 (100 μM, 250 μL, 25 nmol) (Figure 7a). As shown in Figure 7b, the mice being treated with **ZnPc-2NO**-sensitized PDT exhibited significantly slower tumor growth when compared to the PBS-treated mice. At the end of the experiment (on day 20), the tumor volume of the **ZnPc-2NO**-treated mice was significantly smaller than that of the control group (Figure 7c). No noticeable change in the body weight of the mice was observed over the course of treatment (Figure 7d), indicating that PDT with **ZnPc-2NO** did not cause systemic cytotoxicity to the mice.

To further investigate the PDT-stimulated antitumor immune response, we first examined the immune cell populations in the draining lymph nodes by flow cytometry. The proportion of leukocytes in **ZnPc-2NO**-sensitized PDT treatment group was found to be higher compared to the PBS-treated control group, suggesting a robust systemic immune activation. However, while there appeared to be an increase in other types of immune cells, including neutrophils, macrophages, and NK cells, these trends did not reach statistical significance due to the high variances (Figure 8a–d). Since our in vitro studies indicated a key role of DCs in mediating the PDT-induced immune response, we further evaluated the population of myeloid DCs (mDCs) and plasmacytoid DCs (pDCs) in both the lymph nodes and tumor site. As shown in Figure 8e and 8f, while the proportion of mDCs remained unchanged in both the lymph nodes and tumor, the proportion of pDCs, which are the major producer of type I IFN, was significantly increased in the tumor region after PDT. We then examined the adaptive immune response by assessing the proportion of B and T lymphocytes in both the lymph nodes and tumor. As shown in Figure 8g, the proportion of B cells was significantly higher in the lymph nodes of the PDT-treated mice as compared to the control group, indicating an enhanced B lymphocyte recruitment.

As T cells are the key mediators of antitumor function in cancer immunotherapy,[37] the levels of several types of T cells in the tumor after the PDT treatment with **ZnPc-2NO** were also determined and compared with those of the PBS control. It was found that for the $CD3^+$ T cells (or total T cells), $CD4^+$ T cells (or helper T cells), $CD8^+$ T cells (or cytotoxic T cells), and regulatory T cells (Tregs), the levels

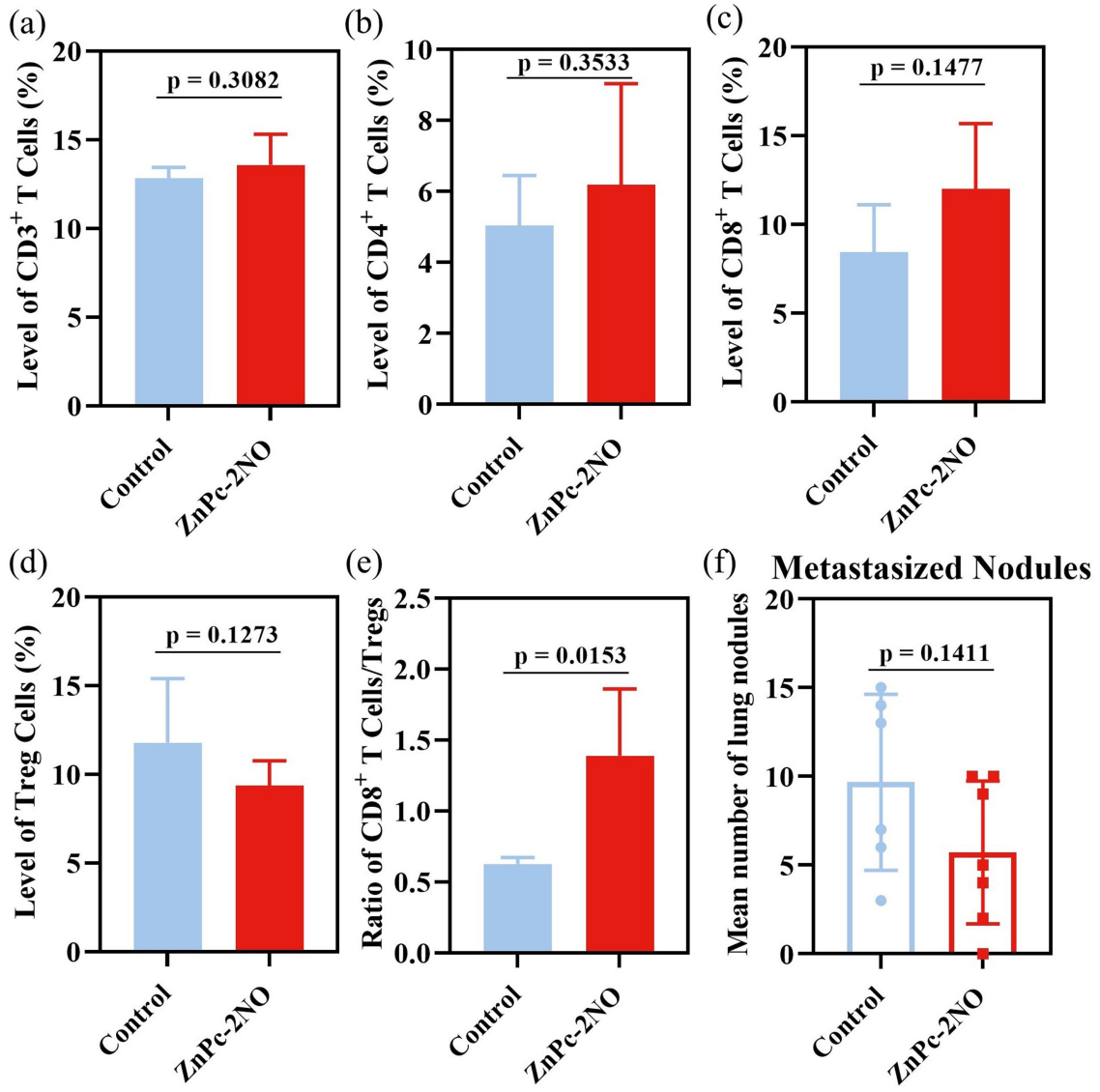

Figure 9. Populations of various T cells in the tumor site on day 20, including (a) $CD3^+$ T cells, (b) $CD4^+$ T cells, (c) $CD8^+$ T cells, and (d) Tregs. (e) The ratio of $CD8^+$ T cells to Tregs. (f) Mean number of metastasized lung nodules on day 20. The statistical analysis of the p-value is also shown in each figure.

for the treatment and control groups were not significantly different (Figure 9a–d). As one of the primary tumor-infiltrating immune cell types, $CD8^+$ T cells play a crucial role in the immune response by identifying and killing cancer cells.[38] A higher number of these cells is generally associated with a stronger immune response. On the other hand, Tregs are a subset of T cells that modulate the immune system, maintain tolerance to self-antigens, and prevent autoimmune diseases by suppressing or downregulating the induction and proliferation of effector T cells. The ratio of $CD8^+$ T cells to Tregs can provide valuable insight into the balance of immune activation and suppression. A higher ratio (i.e., more $CD8^+$ T cells relative to Tregs) is often associated with a more robust immune response. Conversely, a lower ratio (i.e., fewer $CD8^+$ T cells relative to Tregs) indicates a suppressed immune response. This ratio is being recognized as a reliable marker for anti-tumor immune response.[39] Therefore, we calculated this ratio and found that the value was significantly increased in the **ZnPc-2NO**-treated tumors (Figure 9e). These results indicated that **ZnPc-2NO**-mediated PDT promoted significant changes in the immune landscape at the tumor site and the draining lymph nodes. Finally, the anti-metastatic effect of **ZnPc-2NO**-mediated PDT was examined by evaluating the extent of lung metastasis. We observed a downward trend in the number of lung nodules in PDT-treated mice, though the difference did not reach statistical significance (Figure 9f). Overall, our results showed that the **ZnPc-2NO**-mediated PDT potently suppressed tumor growth and elicited a robust antitumor immune response in vivo.

Conclusion

In summary, we designed, synthesized, and characterized two novel NO-releasing phthalocyanines, namely **ZnPc-2NO** and **ZnPc-4NO**. Upon interaction with the intracellular GSH, they released NO that could inhibit the cellular respiration and downregulate the HIF-1α protein level, relieving hypoxia in HT29 and A549 cells. Upon light irradiation, both compounds exhibited high cytotoxicity under both normoxic and hypoxic conditions, demonstrating their ability for oxygen-economized PDT. The comparable photocytotoxicity of **ZnPc-2NO** and **ZnPc-4NO** suggested that two NO donors per a ZnPc core are sufficient for suppressing cellular respiration. Interestingly, **ZnPc-2NO** could also trigger ICD and the release of DAMPs in HT29 cells upon photosensitization, leading to the maturation of DCs and upregulation of antitumor cytokines. In addition, the **ZnPc-2NO**-mediated PDT could suppress tumor growth in 4T1 tumor-bearing mice and induce the recruitment of leukocytes and B cells into the lymph nodes and pDCs in the tumor. The overall results showed that **ZnPc-2NO**-mediated PDT is an effective strategy that can overcome tumor hypoxia and induce ICD, which can activate a robust antitumor immune response.

Acknowledgements

P.C.L. acknowledges the financial support from the Research Grants Council of the Hong Kong Special Administrative Region (Ref. No. CityU 11314522) and City University of Hong Kong (Ref. No. 7005744). K.T.C. also thanks to the support of Croucher Foundation (Ref. No. 9509002 and 9500032), The Science and Technology Innovation Committee of Shenzhen Municipality (Ref. No. JCYJ20210324133813036), Hong Kong Research Grants Council (Ref. No. C7008-22G and 11103523), Tung's Biomedical Sciences Centre (Ref. No. 9609306), and City University of Hong Kong (Ref. No. 7005313, 7005518, 7005740, and 7005873).

Conflict of Interest

The authors declare no conflict of interest.

Data Availability Statement

The data that support the findings of this study are available from the corresponding author upon reasonable request.

Keywords: immunogenic cell death · nitric oxide · phthalocyanines · photodynamic therapy · tumor hypoxia

[1] J. F. Algorri, M. Ochoa, P. Roldán-Varona, L. Rodríguez-Cobo, J. M. López-Higuera, *Cancers* **2021**, *13*, 4447.
[2] a) B. M. Luby, C. D. Walsh, G. Zheng, *Angew. Chem. Int. Ed.* **2019**, *58*, 2558–2569; b) P. Gierlich, A. I. Mata, C. Donohoe, R. M. M. Brito, M. O. Senge, L. C. Gomes-da-Silva, *Molecules* **2020**, *25*, 5317; c) D. Lee, S. Kwon, S.-y. Jang, E. Park, Y. Lee, H. Koo, *Bioactive Mater.* **2022**, *8*, 20–34; d) S. Li, F. Yang, Y. Wang, T. Du, X. Hou, *Chem. Eng. J.* **2023**, *451*, 138621.
[3] T. C. Pham, V.-N. Nguyen, Y. Choi, S. Lee, J. Yoon, *Chem. Rev.* **2021**, *121*, 13454–13619.
[4] a) S. Mallidi, S. Anbil, A.-L. Bulin, G. Obaid, M. Ichikawa, T. Hasan, *Theranostics* **2016**, *6*, 2458–2487; b) R. V. Huis in't Veld, J. Heuts, S. Ma, L. J. Cruz, F. A. Ossendorp, M. J. Jager, *Pharmaceutica* **2023**, *15*, 330.
[5] a) N. C. Denko, *Nat. Rev. Cancer* **2008**, *8*, 705–713; b) D. M. Gilkes, G. L. Semenza, D. Wirtz, *Nat. Rev. Cancer* **2014**, *14*, 430–439.
[6] a) X. S. Li, N. Kwon, T. Guo, Z. Liu, J. Yoon, *Angew. Chem. Int. Ed.* **2018**, *57*, 11522–11531; b) L. Larue, B. Myrzakhmetov, A. Ben-Mihoub, A. Moussaron, N. Thomas, P. Arnoux, F. Baros, R. Vanderesse, S. Acherar, C. Frochot, *Pharmaceuticals* **2019**, *12*, 163; c) L. Huang, S. Zhao, J. Wu, L. Yu, N. Singh, K. Yang, M. Lan, P. Wang, J. S. Kim, *Coord. Chem. Rev.* **2021**, *438*, 213888; d) Z. Shen, Q. Ma, X. Zhou, G. Zhang, G. Hao, Y. Sun, J. Cao, *NPG Asia Mater.* **2021**, *13*, 39.
[7] a) Y. Cheng, H. Cheng, C. Jiang, X. Qiu, K. Wang, W. Huan, A. Yuan, J. Wu, Y. Hu, *Nat. Commun.* **2015**, *6*, 8785; b) Z. Luo, M. Zheng, P. Zhao, Z. Chen, F. Siu, P. Gong, G. Gao, Z. Sheng, C. Zheng, Y. Ma, L. Cai, *Sci. Rep.* **2016**, *6*, 23393; c) Z. Chen, L. Liu, R. Liang, Z. Luo, H. He, Z. Wu, H. Tian, M. Zheng, Y. Ma, L. Cai, *ACS Nano* **2018**, *12*, 8633–8645.
[8] a) S.-Y. Li, H. Cheng, B.-R. Xie, W.-X. Qiu, J.-Y. Zeng, C.-X. Li, S.-S. Wan, L. Zhang, W.-L. Liu, X.-Z. Zhang, *ACS Nano* **2017**, *11*, 7006–7018; b) J. Kim, H. R. Cho, H. Jeon, D. Kim, C. Song, N. Lee, S. H. Choi, T. Hyeon, *J. Am. Chem. Soc.* **2017**, *139*, 10992–10995; c) W. Zhang, S. Li, X. Liu, C. Yang, N. Hu, L. Dou, B. Zhao, Q. Zhang, Y. Suo, J. Wang, *Adv. Funct. Mater.* **2018**, *28*, 1706375; d) J. Bai, X. Jia, W. Zhen, W. Cheng, X. Jiang, *J. Am. Chem. Soc.* **2018**, *140*, 106–109; e) S. Z. F. Phua, G. Yang, W. Q. Lim, A. Verma, H. Chen, T. Thanabalu, Y. Zhao, *ACS Nano* **2019**, *13*, 4742–4751; f) Y. Li, P. Sun, L. Zhao, Z. Yan, D. K. P. Ng, P.-C. Lo, *Angew. Chem. Int. Ed.* **2020**, *59*, 23228–23238; g) Y. Hu, X. Wang, P. Zhao, H. Wang, W. Gu, L. Ye, *Biomater. Sci.* **2020**, *19*, 2931–2938; h) L. He, F. Xu, Y. Li, H. Jin, P.-C. Lo, *Acta Biomater.* **2023**, *162*, 51–71.
[9] a) W. Y. Yu, T. Liu, M. K. Zhang, Z. X. Wang, J. J. Ye, C. X. Li, W. L. Liu, R. Q. Li, J. Feng, X. Z. Zhang, *ACS Nano* **2019**, *13*, 1784–1794; b) Q. Xiang, B. Qiao, Y. Luo, J. Cao, K. Fan, X. Hu, L. Hao, Y. Cao, Q. Zhang, Z. Wang, *Theranostics* **2021**, *11*, 1953–1969; c) Y. Zhang, P. Zhao, X. Chen, C. Xu, J. Guo, X. Qu, X. Hu, H. Gao, P. Huang, J. Zhang, *ACS Appl. Mater. Interfaces* **2023**, *15*, 12750–12765.
[10] J.-Q. Huang, L.-P. Zhao, X. Zhou, L.-S. Liu, R.-R. Zheng, F.-A. Deng, Y.-B. Liu, X.-Y. Yu, S.-Y. Li, H. Cheng, *Small* **2022**, *18*, 2107467.
[11] a) L.-P. Zhao, R.-R. Zheng, H.-Q. Chen, L.-S. Liu, X.-Y. Zhao, H.-H. Liu, X.-Z. Qiu, X.-Y. Yu, H. Cheng, S.-Y. Li, *Nano Lett.* **2020**, *20*, 2062–2071; b) P. Yuan, F.-A. Deng, Y.-B. Liu, R.-R. Zheng, X.-N. Rao, X.-Z. Qiu, D.-W. Zhang, X.-Y. Yu, H. Cheng, S.-Y. Li, *Adv. Healthcare Mater.* **2021**, *10*, 2100198; c) X. Li, H. Wang, Z. Li, D. Li, X. Lu, S. Ai, Y. Dong, S. Liu, J. Wu, W. Guan, *Biomaterials* **2022**, *26*, 47.
[12] M. Li, Y. Shao, J. H. Kim, Z. Pu, X. Zhao, H. Huang, T. Xiong, Y. Kang, G. Li, K. Shao, J. Fan, J. A. Foley, J. S. Kim, X. Peng, *J. Am. Chem. Soc.* **2020**, *142*, 5380–5388.
[13] Z. Yang, J. Wang, S. Liu, X. Li, L. Miao, B. Yang, C. Zhang, J. He, S. Ai, W. Guan, *Biomaterials* **2020**, *229*, 119580.
[14] J. Yu, Q. Li, Z. Wei, G. Fan, F. Wan, L. Tian, *Acta Biomater.* **2023**, *170*, 330–343.

[15] I. Vercellino, L. A. Sazanov, *Nat. Rev. Mol. Cell Biol.* **2022**, *23*, 141–161.
[16] J. T. Coates, M. Skwarski, G. S. Higgins, *Br. J. Radiol.* **2019**, *92*, 20170843.
[17] G. C. Brown, V. Borutaite, *Free Radical Biol. Med.* **2002**, *33*, 1440–1450.
[18] P. G. Wang, M. Xian, X. Tang, X. Wu, Z. Wen, T. Cai, A. J. Janczuk, *Chem. Rev.* **2002**, *102*, 1091–1134.
[19] P.-C. Lo, M. S. Rodriguez-Morgade, P. K. Pandey, D. K. P. Ng, T. Torres, F. Dumoulin, *Chem. Soc. Rev.* **2020**, *49*, 1041–1056.
[20] C. Farren, C. A. Christensen, S. Fitz Gerald, M. R. Bryce, A. Beeby, *J. Org. Chem.* **2002**, *67*, 9130–9139.
[21] G. N. Ziakas, E. A. Rekka, A. M. Gavalas, P. T. Eleftheriou, K. C. Tsiakitzis, P. N. Kourounakis, *Bioorg. Med. Chem.* **2005**, *13*, 6485–6492.
[22] K. Lange, A. Koenig, C. Roegler, A. Seeling, J. Lehmann, *Bioorg. Med. Chem. Lett.* **2009**, *19*, 3141–3144.
[23] S. Zhu, J. Zhang, G. Vegesna, F.-T. Luo, S. A. Green, H. Liu, *Org. Lett.* **2011**, *13*, 438–441.
[24] a) J. C. H. Chu, M. L. Chin, C. T. T. Wong, M. Hui, P.-C. Lo, D. K. P. Ng, *Adv. Ther.* **2021**, *4*, 2000204; b) L. K. B. Tam, L. Yu, R. C. H. Wong, W.-P. Fong, D. K. P. Ng, P.-C. Lo, *J. Med. Chem.* **2021**, *64*, 17455–17467.
[25] L. K. B. Tam, J. C. H. Chu, L. He, C. Yang, K.-C. Han, P. C. K. Cheung, D. K. P. Ng, P.-C. Lo, *J. Am. Chem. Soc.* **2023**, *145*, 7361–7375.
[26] Z. Weiszhár, J. Czúcz, C. Révész, L. Rosivall, J. Szebeni, Z. Rozsnyay, *Eur. J. Pharm. Sci.* **2012**, *45*, 492–498.
[27] J. Sun, X. Zhang, M. Broderick, H. Fein, *Sensor* **2003**, *3*, 276–284.
[28] J.-Z. Sheng, D. Wang, A. P. Braun, *J. Pharmcol. Exp. Ther.* **2005**, *315*, 931–940.
[29] C.-T. Chiang, R. Lau, A. Ghaffarizadeh, M. Brovold, D. Vyas, E. F. Juárez, A. Atala, D. B. Agus, S. Soker, P. Macklin, D. Ruderman, S. M. Mumenthaler, *GigaScience* **2021**, *10*, giab026.
[30] K. Yao, J. A. Gietema, S. Shida, M. Selvakumaran, X. Fonrose, N. B. Haas, J. Testa, P. J. O'Dwyer, *Br. J. Cancer* **2005**, *93*, 1356–1363.
[31] L. Korrodi-Gregório, V. Soto-Cerrato, R. Vitorino, M. Fardilha, R. Pérez-Tomás, *PLoS One* **2016**, *11*, e0165973.
[32] S. Wang, Y. Yan, Z. Cheng, Y. Hu, T. Liu, *Cell Death Discov.* **2018**, *4*, 26.
[33] X. Liu, K. Shan, X. Shao, X. Shi, Y. He, Z. Liu, J. A. Jacob, L. Deng, *Int. J. Nanomed.* **2021**, *16*, 753–761.
[34] a) A. D. Garg, D. V. Krysko, P. Vandenabeele, P. Agostinis, *Photochem. Photobiol. Sci.* **2020**, *10*, 670–680; b) Y. Lu, W. Sun, J. Du, J. Fan, X. Peng, *JACS Au* **2023**, *3*, 682–699.
[35] P. De Silva, M. A. Saad, H. C. Thomsen, S. Bano, S. Ashraf, T. Hasan, *J. Porphyrins Phthalocyanines* **2020**, *24*, 1320–1360.
[36] P. De Silva, S. Bano, B. W. Pogue, K. K. Wang, E. V. Maytin, T. Hasan, *Nat. Photonics* **2021**, *10*, 3199–3214.
[37] Z. Zhang, S. Liu, B. Zhang, L. Qiao, Y. Zhang, Y. Zhang, *Front. Cell Dev. Biol.* **2020**, *8*, 17.
[38] S. Kumar, S. K. Singh, B. Rana, A. Rana, *Drug Discov. Today* **2021**, *26*, 951–967.
[39] a) E. Sato, S. H. Olson, J. Ahn, B. Bundy, H. Nishikawa, F. Qian, A. A. Jungbluth, D. Frosina, S. Gnjatic, C. Ambrosone, J. Kepner, T. Odunsi, G. Ritter, S. Lele, Y.-T. Chen, H. Ohtani, L. J. Old, K. Odunsi, *Proc. Natl. Acad. Sci. USA* **2005**, *102*, 18538–18543; b) H. Wang, X. Han, Z. Dong, J. Xu, J. Wang, Z. Liu, *Adv. Funct. Mater.* **2019**, *29*, 1902440; c) S. Kim, J. Koh, S. G. Song, J. Yim, M. Kim, B. Keam, Y. T. Kim, J. Kim, D. H. Chung, Y. K. Jeon, *BMC Cancer* **2022**, *22*, 1120.

Manuscript received: March 6, 2024
Accepted manuscript online: June 18, 2024
Version of record online: August 12, 2024